Biosensors and Bioelectronics 126 (2019) 448–454

Contents lists available at ScienceDirect

Biosensors and Bioelectronics

journal homepage: www.elsevier.com/locate/bios

Dual mode competitive electrochemical immunoassay for B-type natriuretic peptide based on GS/SnO_2/polyaniline-Au and $ZnCo_2O_4$/N-CNTs

Xuan Li, Li Liu, Xue Dong, Guanhui Zhao, Yueyuan Li, Juncong Miao, Jinglong Fang, Min Cui, Qin Wei, Wei Cao*

Key Laboratory of Interfacial Reaction & Sensing Analysis in Universities of Shandong, School of Chemistry and Chemical Engineering, University of Jinan, Jinan 250022, PR China

ARTICLE INFO

Keywords:
Dual mode
Competitive electrochemical immunosensor
$ZnCo_2O_4$ quantum dots
N-doped carbon nanotubes

ABSTRACT

A sensitive dual mode competitive electrochemical immunosensor for the detection of B-type natriuretic peptide (BNP) was successfully fabricated, which based on differential pulse voltammetry (DPV) and amperometric *i-t* curve response modes. Polyaniline (PAN) and tin dioxide (SnO_2) were loaded on graphene sheets (GS), which could effectively promote the electron transfer process, thereby amplifying the current signal and increasing the sensitivity of the immunosensor. To promote biocompatibility, gold nanoparticles (Au) were incorporated on GS/SnO_2/PAN (GS/SnO_2/PAN-Au). GS/SnO_2/PAN-Au complex was gotten to act as the platform which could provide a clearly DPV signals. N-doped carbon nanotubes (N-CNTs) embellished by $ZnCo_2O_4$ quantum dots ($ZnCo_2O_4$/N-CNTs) with excellent catalytic properties for the reduction of H_2O_2 was gotten to act as the label of the antibody-BNP (Ab), providing an obviously current signal through amperometric *i-t* curve method. A large quantity of BNP could be stable loaded in the modified electrode via GS/SnO_2/PAN-Au with excellent electrical conductivity and good biocompatibility, which could compete with target-BNP to combine Ab that labelled by $ZnCo_2O_4$/N-CNTs. Under the optimum conditions, the immunosensor exhibited remarkable analytical performance of a linear range from 0.01 pg/mL to 1 ng/mL with a detection limit of 3.4 fg/mL for quantitative detection of BNP (S/N = 3). This method was able to become a universal strategy for other biological detection.

1. Introduction

Cardiovascular disease is the important causes of people death in many countries. Heart failure (HF) is one of the most important clinical manifestations of this disease (Lei et al., 2017). B-type natriuretic peptide (BNP) was discovered in 1988 which has become an internationally recognized biomarker in the diagnosis of HF (de Ávila et al., 2013; Serafín et al., 2018). BNP which composed of 32 amino acids and distributed in the brain, heart, spinal cord and other parts is a kind of short peptide hormone synthesized which secreted by cardiomyocytes (Saito et al., 1989).

In recent years, there are many methods for detecting BNP, of which fluorescence immunoassay has been used to detect BNP in clinical practice. However, this method is time-consuming, complicated in operation and expensive in equipment. (Lei et al., 2017; R. Liu et al., 2010). The surface plasmon resonance (SPR) method has been used to directly detect BNP with a low detection limit, unfortunately, this is unfitted for bedside monitoring due to the system needs relatively high power and an expensive excitation light source and photomultiplier (Jang et al., 2014; Kurita et al., 2006). Therefore, fabricating a capable biosensor of detecting BNP with high sensitivity, high specificity, simple operation and price moderate is essential. Electrochemical immunosensor based on specific binding between antigens and antibodies have achieved widespread concern in virtue of the advantages about high sensitivity, low detection limit, high specificity and high response speed (Liu et al., 2017; Wang et al., 2015). Dual mode characteristics of electrochemical immunosensor can improve clinical reliability and analytical performance (Wei et al., 2017).

Graphene sheets (GS) is a two-dimensional honeycomb lattice stacked from a single layer of carbon atoms with a large specific surface area (Fan et al., 2016), favorable chemical properties and excellent conductivity (Dong et al., 2017), which has been broad used due to unique nanostructures in the field of nanoelectronics (Xiong et al., 2018), sensors (Han et al., 2018), energy storage devices etc (Choi et al., 2018; Xu et al., 2014). However, when graphene dispersion solutions are dried, GS are prone to aggregation due to Van der Waals and π-π stacking interactions among individual GS (J. Liu et al., 2010). The aggregation problem of GS could be minimized or prevented by

* Corresponding author.
E-mail addresses: jncw88@163.com, jn_chm302@163.com (W. Cao).

https://doi.org/10.1016/j.bios.2018.11.009
Received 4 June 2018; Received in revised form 4 October 2018; Accepted 7 November 2018
Available online 09 November 2018
0956-5663/

incorporation of nanoparticles into GS (Si and Samulski, 2008). Many nanomaterials decorated GS have recently been reported including SnO_2 nanoparticles which have the advantage of excellent optical and electrical properties (Tran et al., 2017), high electron mobility (Ke et al., 2015) and outstanding thermal stability (Jin and Jia, 2015). Simultaneously, the electrochemical performance are optimized because of the synergetic effect between them (Song et al., 2011). Polyaniline (PAN) is a distinctive conductive polymer which is able to improve the electron transfer (J. Wang et al., 2017). In-situ formation of PAN on graphene/SnO_2 (GS/SnO_2) is in a position to synthesize sandwich structural composites, which can improve the electrochemical performance of the composite (Li et al., 2016). In addition, gold nanoparticlesis (Au) are able to immobilize the antigen on the electrode surface by Au−NH_2 bonds, increasing the binding rate of the antigen (Y. Wang et al., 2018). In short, the GS/SnO_2/PAN-Au composite as the matrix materials, excellent conductivity and biocompatibility, assist the constructed electrochemical immunosensor to improve the performance.

Mixed transition-metal oxides with a spinel structure have been considered a promising catalytic material, such as $ZnCo_2O_4$ have excellent catalytic properties for the reduction of H_2O_2, due to the synergistic effects where metal oxides with high oxidation states play the part of oxidants and another with high conductivity play the part of electron donors (Shiqiang et al., 2017). Quantum dots possess advantages of high specific surface area, sufficient active sites and short electron transfer pathways, which can further improve the utilization and electrochemical performance accordingly of materials (Ma et al., 2017). Carbon nanotubes (CNTs), as a well-known one-dimensional nanomaterial, are widely used for modifying electrode surface thanks to their large surface area, high electronic conductivity and stable mechanical properties (Y. Liu et al., 2016; Y. Wang et al., 2017a). Furthermore, N-doped carbon nanotubes (N-CNTs) not only have rich active sites but also improve the stability and electrocatalytic activity of metal oxides. (L. Liu et al., 2016; Z.Q. Liu et al., 2016). Accordingly, N-CNTs embellished by $ZnCo_2O_4$ quantum dots ($ZnCo_2O_4$/N-CNTs) can enhance the catalytic properties of the label greatly.

In this work, a large amount of BNP was immobilized on the electrode modified with GS/SnO_2/PAN-Au composite, after another the nonspecific site was blocked via BSA. The electrode was then modified with a mixed solution of target-BNP and the antibody-BNP (Ab) that labelled by $ZnCo_2O_4$/N-CNTs ($ZnCo_2O_4$/N-CNTs-Ab). By this way, the immobilized BNP and the target-BNP would compete against each other to acquire the $ZnCo_2O_4$/N-CNTs-Ab to determination of the target-BNP via changes in electrochemical signals. All in all, the work not only utilized the GS/SnO_2/PAN-Au composite to provide electrochemical signals through differential pulse voltammetry (DPV) method, but also offered the amperometric *i–t* curve signal by utilizing the $ZnCo_2O_4$/N-CNTs material. As a result, the competitive and dual mode property of electrochemical immunosensor was responsible for an interaction with GS/SnO_2/PAN-Au and $ZnCo_2O_4$/N-CNTs complex in the detection of BNP on the basis of two different electrochemical signals change, increasing analytical performance, hence improving the accuracy of the results and clinical reliability.

2. Experimental section

2.1. Reagents and apparatuses

Graphite powder was purchased from Sinogharm Chenical Reagent Co., Lid (Shanghai, China). Tin (IV) chloride pentahydrate ($SnCl_4{\cdot}5H_2O$) and other solid reagents were purchased from Macklin Biochemical Co., Ltd (Shanghai, China). N,N-Dimethylformamide (DMF) and aniline were obtained from fuyu Fiine Chemical Co., Ltd (Tianjin,China). $HAuCl_4{\cdot}4H_2O$, N-hydroxysuccinimide (NHS) and 1-ethyl-3-(3-dimethylaminopropyl) carbodiimide hydrochloride (EDC) were purchased from Aladdin Reagent Database Inc. (Shanghai, China). Bovine serum albumin (BSA) was purchased from Sigma-Aldrich (Beijing, China). Antigen-BNP and antibody-BNP were all obtained from Shanghai Linc-Bio Science Co., Ltd (Shanghai, China).

Scanning electron microscope (SEM) was obtained from a field emission SEM (Zeiss, Germany). Transmission electron microscopic (TEM) image was obtained from a JEOL1400 microscope (Japan). The Fourier transform infrared spectroscopy (FTIR) spectrum was obtained from a VERTEX 70 spectrometer (Bruker, Germany). X-ray diffraction (XRD) patterns were obtained using D8 focus diffractometer (Bruker AXS, Germany). Electrochemical measurements were performed on a CHI760D electrochemical workstation (Chenhua Instrument Shanghai Co., Ltd., China).

2.2. Preparation of $ZnCo_2O_4$/N-CNTs-Ab labels

The synthesis of $ZnCo_2O_4$/N-CNTs adopted a well-known approach (Z.Q. Liu et al., 2016), and the steps were described in the Supplementary materials.

The $ZnCo_2O_4$/N-CNTs was dissolved in 1.9 mL of PBS, and then added 0.5 mL of NHS (2 mmol/L) and 0.5 mL of EDC (10 mmol/L). In addition, 100 μL of Ab (0.5 μg/mL) was added to the resulting solution and shaken for 12 h at a low temperature of 4 °C. Finally, the solution was centrifuged at 4 °C, washed with PBS, and the resulting solid was dissolved in 1 mL of PBS.

2.3. Preparation of electrochemical immunosensor

Fig. 1 shows the schematic diagram of the dual mode competitive electrochemical immunosensor. In the first place, the GCE was polished with alumina powder, and then the GCE was washed with deionized water to wash off the excess alumina powder after modify the electrode. In the second step, 10 μL GS/SnO_2/PAN-Au (1.5 mg/mL) was dropped on the pretreated electrode surface and dried at room temperature for 1 h. In the third part, 10 μL BNP (1 μg/mL) was incubated onto the modified electrodes, after incubated, the excess BNP was washed off with buffer solution. And then 5 μL BSA (1%) was modified on the electrode to block the nonspecific site. After drying, the excess BSA was washed off with buffer solution. In the meantime, the nonspecific sites of $ZnCo_2O_4$/N-CNTs-Ab was blocked with BSA, afterwards it was mixed with the target-BNP in an equal volume to prepare for use. Finally, 10 μL of a mixed solution of $ZnCo_2O_4$/N-CNTs-Ab and target-BNP was dispensed onto the surface of modified electrode. After incubated, the

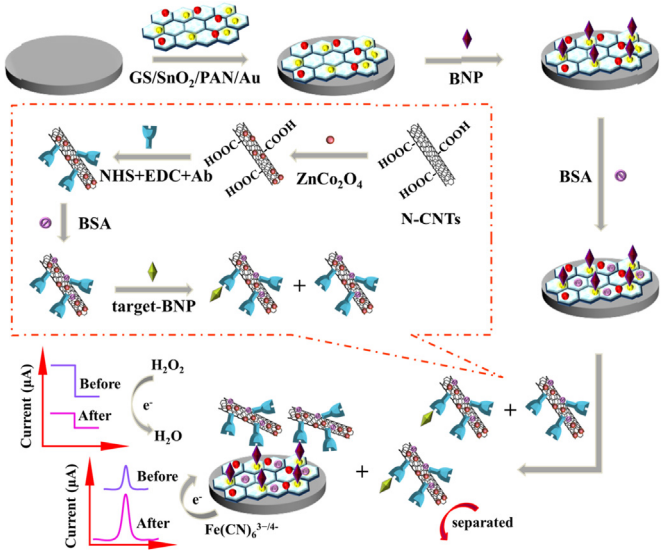

Fig. 1. The schematic illustration of the dual mode competitive electrochemical immunosensor.

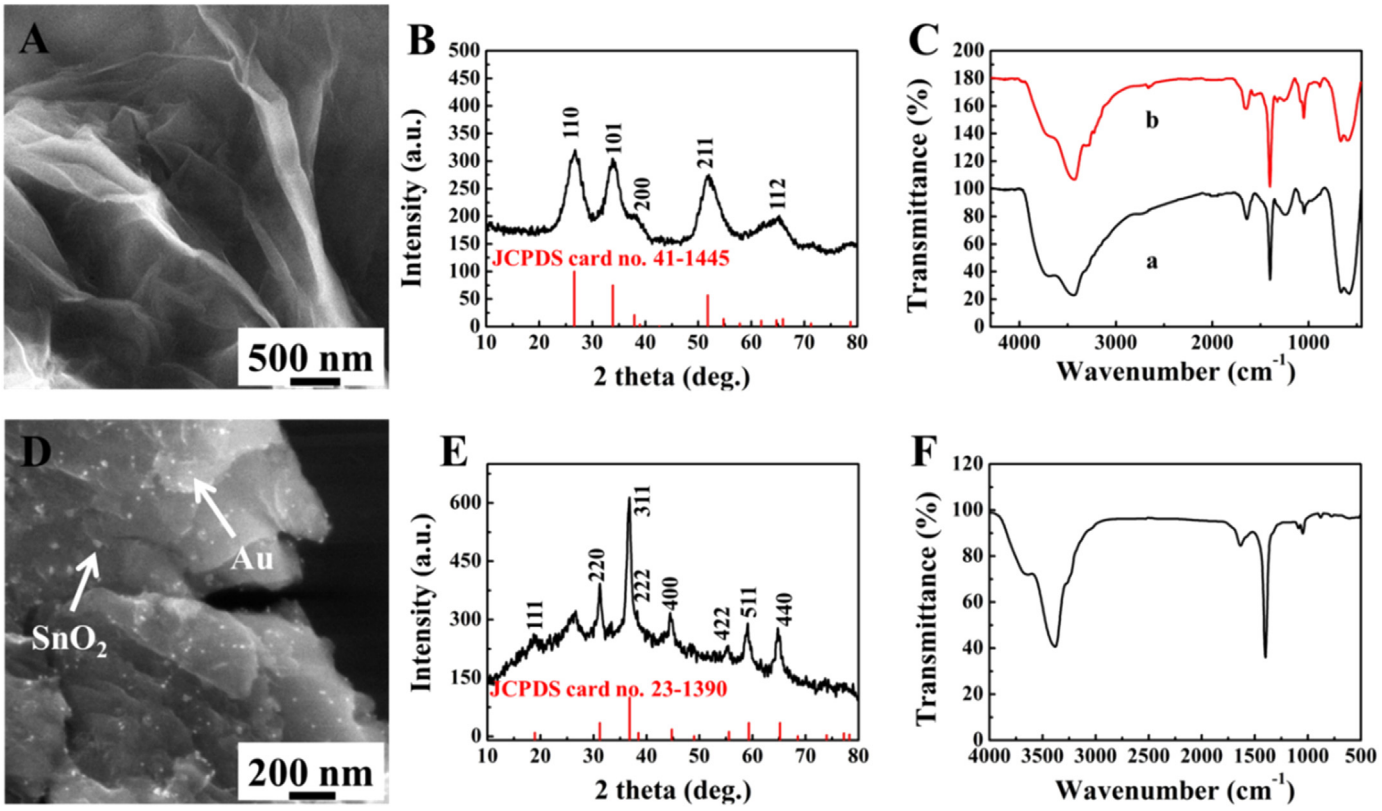

Fig. 2. (A) SEM image of GS; (B) XRD pattern of GS/SnO_2; (C) FTIR spectrum of GS/SnO_2 (a) and GS/SnO_2/PAN (b); (D) SEM image of GS/SnO_2/PAN-Au; (E) XRD pattern of $ZnCo_2O_4$/N-CNTs; (F) FTIR spectrum of N-CNTs.

electrode washed with buffer solution. The final electrode was subjected to electrochemical measurements including DPV method and amperometric *i–t* curve method. DPV was recorded (range and direction: from −0.2 to 0.6 V, increase: 0.004 V, amplitude: 0.05 V, pulse width: 0.05 s, sampling width: 0.0167 s, pulse period: 0.5 s) in PBS containing 5 mmol/L $K_3[Fe(CN)_6]$ (pH = 6.8). Amperometric *i–t* curve was performed by scanning the potential at − 0.4 V in PBS (10 mL, pH = 6.8) injecting 5 mol/L H_2O_2 (10 μL).

3. Results and discussion

3.1. The morphologies of materials

Fig. 2 (A, B) illustrates the images of the GS and GS/SnO_2. The inset of Fig. 2B shows the XRD pattern of the GS/SnO_2, the distinct peaks at 2θ = 26.6°, 33.9°, 37.9°, 51.8° and 64.7°, corresponding to the tetragonal rutile structure (110), (101), (200), (211), and (112) of SnO_2 (JCPDS card no. 41-1445). The broadened diffraction peaks testify to the small crystallite size of SnO_2. There are no obvious peaks corresponding to GS in the pattern, that on account of: (1) disordered interfacial structure due to the interfacial bonding between SnO_2 and GS; (2) The small quantity of GS in the composites; (3) The disordered stacking properties of GS in the composites (Song et al., 2011). As seen from Fig. S1, GS is obviously loaded with solid nanoparticles, which shows that we succeeded in loading SnO_2 on GS (Supplementary materials). Moreover, SnO_2 nanoparticles, the most of which ranges from 30 nm to 40 nm in size, are well dispersed on the surface of GS. Besides, the FTIR spectrum proves the above statement (Fig. 2C). For GS/SnO_2 (a), the peak at 3440 cm^{-1} represents the stretching vibrations of O—H, C—O stretching at 1400 cm^{-1}, the peak range of 500–750 cm^{-1} are caused by the symmetric stretching of Sn—O—Sn, C—O—C and C—O deformation are also observed at 1244 cm^{-1} and 1065 cm^{-1}, proving the existence of GS and SnO_2 (Bera et al., 2018; Wu et al., 2017). As shown in Fig. 2C (b), the characteristic peaks including C-C stretching at 800 cm^{-1}, C—N stretching at 1310 cm^{-1} and C=C stretching at 1560 cm^{-1} explain that PAN is synthesized successfully in GS/SnO_2/PAN (Acevedo et al., 2011; Mishra and Ramaprabhu, 2011). As revealed in the SEM of GS/SnO_2/PAN-Au (Fig. 2D), a number of bright spheres which average size is 17 nm could be observed clearly on the surface of composite, confirming that the Au nanoparticles is dispersed on the surface of GS/SnO_2/PAN. The spinel crystal plane of $ZnCo_2O_4$ is also identified by the XRD pattern of $ZnCo_2O_4$/N-CNTs (Fig. 2E). The distinct peaks at 2θ = 18.9°, 31.3°, 36.8°, 38.5°, 44.7°, 55.6°, 59.3°, and 65.1° respectively, corresponding to (111), (220), (311), (222), (400), (422), (511), and (440), which diffraction peaks can vest in the $ZnCo_2O_4$ phase (JCPDS card no. 23-1390) (Shiqiang et al., 2017). In addition, the presence of N-CNTs is corroborated by the signal presenting at 2θ of 26.4° (Fig. S2), which roots in the (002) graphitic diffraction of the CNTs structure (Z.Q. Liu et al., 2016). Fig. S3 reveals the TEM images of $ZnCo_2O_4$/N-CNTs, it can be clearly observed that there are a large number of quantum dots deposited on N-CNTs, from which demonstrating the $ZnCo_2O_4$ is grew on N-CNTs. Furthermore, the FTIR spectrum is used for recording the functional group of N-CNTs (Fig. 2F), O—H stretching at 3400 cm^{-1}, O—H bending at 1400 cm^{-1} and C—O stretching at 1630 cm^{-1}, indicating the −COOH group is existed on the surface of N-CNTs (Hu et al., 2017). The existence of −COOH functional group is beneficial for the combination of the $ZnCo_2O_4$/N-CNTs with Ab.

3.2. Mechanism of signal amplification strategy

The dual mode competitive electrochemical immunoensor has excellent catalytic activity and obviously electrical conductivity because of the synergistic effect with various fabricating materials. In this study, the conductivity of sensor platform was a significant factor for the sensitivity of electrochemical immunosensor. In order to prove the

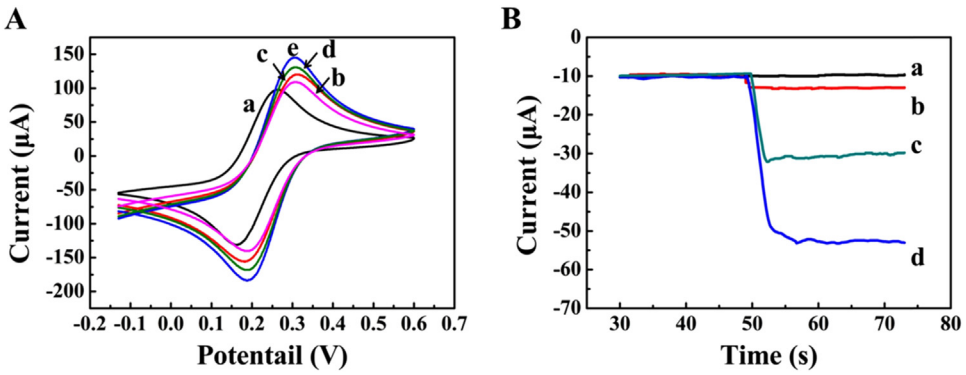

Fig. 3. (A) CV responses of immunosenser for different signal labels in 5 mmol/L $K_3[Fe(CN)_6]$ including GCE (a), GCE/GS (b), GCE/GS/SnO_2 (c), GCE/GS/SnO_2/PAN (d), GCE/GS/SnO_2/PAN-Au (e) and (B) amperometric *i-t* curve responses at –0.4 V in PBS injecting 5 mmol/L H_2O_2 of GCE (a), GCE/N-CNTs (b), GCE/$ZnCo_2O_4$ (c), GCE/$ZnCo_2O_4$/N-CNTs (d).

charge transfer efficiency of GS/SnO_2/PAN-Au composite materials, which were tested by cyclic voltammetry (CV) in 5 mmol/L $K_3[Fe(CN)_6]$. As shown in Fig. 3A, electrochemical response signals of five different materials including GCE (a), GCE/GS (b), GCE/GS/SnO_2 (c), GCE/GS/SnO_2/PAN (d), GCE/GS/SnO_2/PAN-Au (e) were increased orderly, which were attributed to that: firstly, GS has outstanding large specific surface area and electrical conductivity to amplify charge transfer. Secondly, SnO_2 with outstanding chemical and thermal stability was loaded in GS, which can prevent GS from agglomerating. Thirdly, due to the excellent conductivity of PAN as well as Au can improve the electron transfer and biocompatibility, the formation of PAN and Au in situ on GS/SnO_2 composites can improve the electrochemical performance of the material and allow the material to capture massive BNP.

To examine catalytic activity towards the reduction of H_2O_2, the current signal of different materials was compared by using the amperometric *i-t* curve. As shown in Fig. 3B, the bare GCE (a) and other materials including N-CNTs (b), $ZnCo_2O_4$ (c) and $ZnCo_2O_4$/N-CNTs (d) demonstrated different response currents. It can be seen that the bare GCE had no catalytic properties towards the reduction of H_2O_2. However, a scarcely any current signal appears when the N-CNTs were modified on the bare GCE. At the same time, when the bare GCE was modified with GCE/$ZnCo_2O_4$ (c), it showed a more obvious current signal on account of that $ZnCo_2O_4$ quantum dots have the advantages of excellence catalytic properties for the reduction of H_2O_2. Compared with other materials, $ZnCo_2O_4$/N-CNTs had superior catalytic performance for the reduction of H_2O_2. All this conclusively proved that the catalytic activity of $ZnCo_2O_4$/N-CNTs composites is significantly improved depending on that the N-CNTs deposited a large number of $ZnCo_2O_4$ quantum dots and reduced the agglomeration of it.

3.3. Characterization of the immunosensor

A.C. impedance measurement has been considered as one of the most impactful methods to monitor the fabrication process of electrochemical immunosensor (Li et al., 2018). The experiments of A.C. impedance were recorded in 2.5 mmol/L $[Fe(CN)_6]^{3-/4-}$ containing 0.1 mol/L KCl at potential of 0.26 V with frequency range of 0.5–10^5 Hz. As shown in Fig. 4A, it could be obvious that the bare GCE (a), almost in a straight line, displayed superior conductivity. Following that, the GS/SnO_2/PAN-Au arc (b) was closer to the straight line when the composites was modified on the bare GCE, demonstrating the GS/SnO_2/PAN-Au composites had better conductive property than the bare GCE. Subsequently, the semicircle diameters were increased when the BNP (c), BSA (d) and $ZnCo_2O_4$/N-CNTs-Ab (e) were modified on the resultant GCE in turn, which were caused by that the electrons transfer was obstructed by bioactive substances, indicating the modification of electrode was successful.

3.4. Optimization of experimental conditions

It is necessary to optimize experimental conditions including the pH of the PBS, the concentration of GS/SnO_2/PAN-Au and $ZnCo_2O_4$/N-CNTs to achieve optimal electrochemical signal. The immunosensor was applied for detection of BNP at a concentration of 1 pg/mL.

The pH value is one of the important factors that affect the current signal and the activity of biological proteins. As seen from Fig. 4B, the immunosensor exhibited different DPV response at different pH values. The figure shows the current response increased with the variation of pH values from 5.3 to 6.8 and then the signal decreased with the variation of pH values from 6.8 to 9.2, demonstrating the pH values of 6.8 was obtained optimal DPV response. Thus, PBS at the pH value of 6.8 was selected as the optimal electrolyte to test this immunosensor.

Moreover, the concentration of GS/SnO_2/PAN-Au is one of the significant factors affecting the current signal as well. As seen from Fig. 4C, different current signals were generated at different concentrations of GS/SnO_2/PAN-Au by DPV (pH = 6.8). The current signals obviously increased with the concentrations of GS/SnO_2/PAN-Au increasing from 0.5 mg/mL to 1.5 mg/mL. Meanwhile, the current signals decreased slowly with the concentrations of GS/SnO_2/PAN-Au increasing from 1.5 mg/mL to 3.0 mg/mL. It is demonstrated that the increase of GS/SnO_2/PAN-Au concentration lead to increase of immobilization for BNP and electron transfer, yet in high concentrations, the excessively GS/SnO_2/PAN-Au could hinder the electron transfer because of the increased interface resistance. Thus, 1.5 mg/mL GS/SnO_2/PAN-Au was selected as the optimal electrolyte to test this immunosensor.

In addition, the concentration of $ZnCo_2O_4$/N-CNTs is also a vital parameter influencing the value of electrocatalytic current response change. As seen from Fig. 4D, the current signals of employing different concentrations for $ZnCo_2O_4$/N-CNTs as the label in the fabrication of immunosensor towards the reduction of 5 mmol/L H_2O_2 in PBS at pH = 6.8 were display. As shown in this figure, the current signal reached the optimal value with the concentration of $ZnCo_2O_4$/N-CNTs of 2.0 mg/mL. The more $ZnCo_2O_4$/N-CNTs, the more Ab would be captured. But only a certain amount of antibodies can combine with it, so using too much $ZnCo_2O_4$/N-CNTs was useless. Thus, 2.0 mg/mL $ZnCo_2O_4$/N-CNTs was selected as the optimal electrolyte to test this immunosensor.

3.5. Analytical performance

Under the optimal experimental conditions, the relationship between the DPV peak current and the concentration of BNP was investigated. The Fig. 5 (A, B) shows in the range 0.01 pg/mL-1 ng/mL the current signal increased with the increase of BNP concentration. The linear relationship between current signals and the concentrations of BNP was represented by an equation, I_p (μA) = 27.36 + 8.79 lg *[BNP]* (pg/mL) with a correlation coefficient of 0.996. Meanwhile, the amperometric *i-t* curve method about discussing the relationship

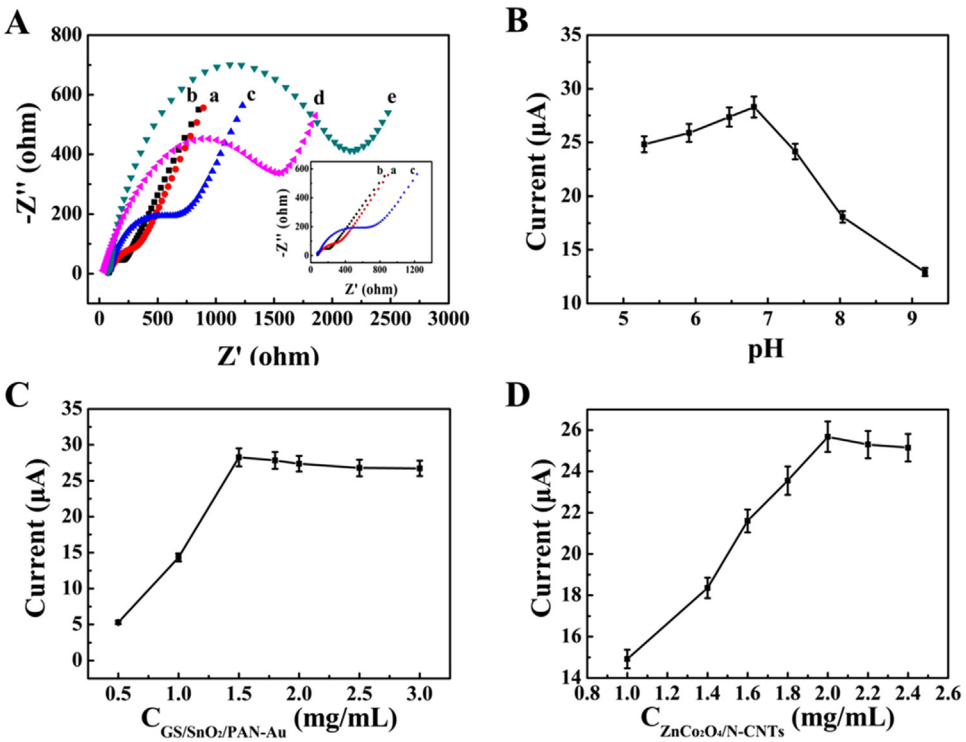

Fig. 4. (A) The Nyquist plots of the A.C. impedance analysis in 2.5 mmol/L $[Fe(CN_6)]^{3-/4-}$ containing 0.1 mol/L KCl at 0.26 V: GCE (a), GCE/GS/SnO_2/PAN-Au (b), GCE/GS/SnO_2/PAN-Au/BNP (c), GCE/GS/SnO_2/PAN-Au/BNP/BSA (d), GCE/GS/SnO_2/PAN-Au/BNP/BSA/$ZnCo_2O_4$/N-CNTs-Ab (e); The optimization of experimental conditions for detection of 1 pg/mL for BNP of pH (B), GS/SnO_2/PAN-Au concentration (C), $ZnCo_2O_4$/N-CNTs (D), error bar = RSD (n = 5).

between the current signal and the concentration of BNP were shown in Fig. 5(C, D). The linear equation was ΔI (μA) = 26.75–6.17 lg*[BNP]* (pg/mL) with a correlation coefficient of 0.995. The limit of detection (LOD) (S/N = 3) was 3.4 fg/mL. As shown in Table S1, the detection method was compared with the previous detection report of BNP, and the designed electrochemical immunosensor had higher sensitivity and lower detection limit. The reasons for this result can be attributed to the following aspects. In the first place, the composite material of GS/SnO_2/PAN-Au with large specific surface area, excellent conductivity and biocompatibility, can effectively promote the electron transfer process, amplify the current signal and provide more binding sites for biomolecules. In the next place, $ZnCo_2O_4$ quantum dots have the advantages of large specific surface area and outstanding catalytic properties for the reduction of H_2O_2. In addition, N-CNTs with abundant active sites, can improve the stability and electrocatalytic activity of metal oxides, which make the-label effectively enhance the catalytic properties, significantly increasing the sensitivity of the immunosensor and reduce the detection limit.

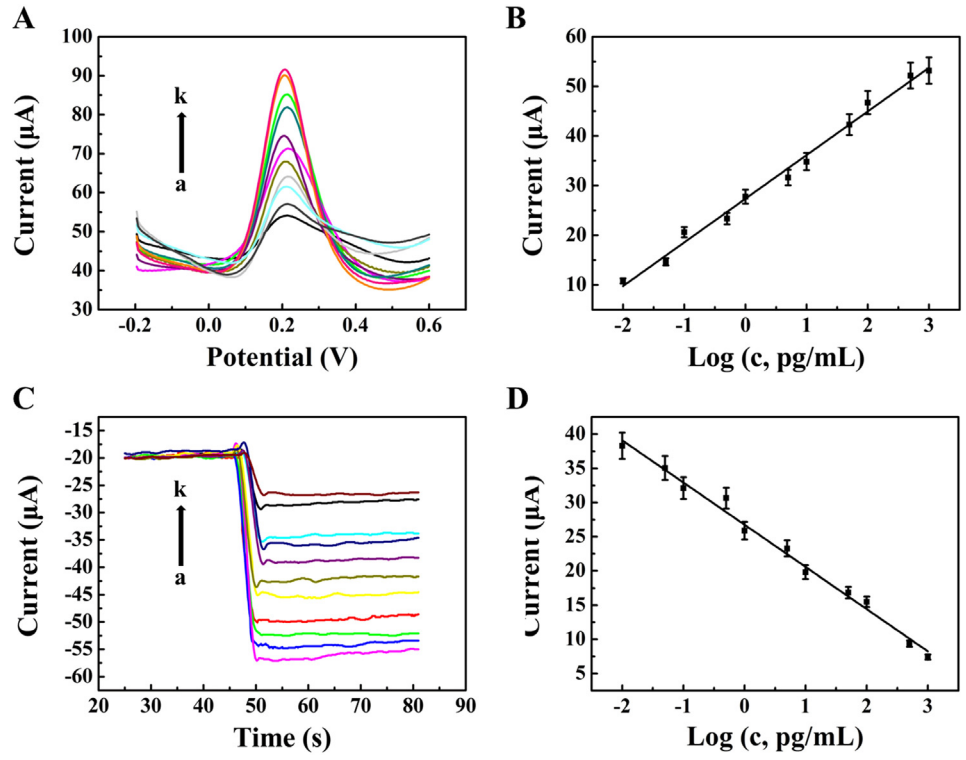

Fig. 5. DPV response (A, B) in PBS containing 5 mmol/L $K_3[Fe(CN)_6]$ and Amperometric *i-t* curve response (C, D) in PBS injecting 5 mmol/L H_2O_2 of the immunosensor for the detection of different concentrations of BNP: (a) 0.01 pg/mL; (b) 0.05 pg/mL;(c) 0.1 pg/mL; (d) 0.5 pg/mL; (e) 1 pg/mL; (f) 5 pg/mL; (g) 10 pg/mL; (h) 50 pg/mL; (i) 100 pg/mL; (j) 500 pg/mL; (k) 1000 pg/mL. Error bar = RSD (n = 5).

Table 1
Determination of BNP in human serum sample.

Serum sample (pg/mL)	Added BNP concentration (pg/mL)	Electrochemical technique	Measured concentration after addition (pg/mL)	Average value (pg/mL)	RSD (%, n = 5)	Recovery (%, n = 5)
20.30	5.00	DPV	25.10, 26.45, 24.15, 25.19	25.20	3.24	97.82
		Amperometric *i-t* curve	24.32, 25.38, 26.19, 25.27	25.27	2.62	99.45
	10.00	DPV	29.33, 30.25, 29.18, 31.33	29.99	2.86	96.98
		Amperometric *i-t* curve	29.31, 30.36, 29.19, 31.50	30.06	3.10	97.62
	15.00	DPV	36.36, 35.75, 33.65, 36.88	35.61	3.45	102.11
		Amperometric *i-t* curve	36.25, 33.80, 36.34, 35.78	35.51	3.28	101.41

3.6. Selectivity, reproducibility and stability of the immunosensor

In order to assess the selectivity of the dual mode competitive electrochemical immunosensors, α-fetoprotein (AFP), carcinoembryonic antigen (CEA), ascorbic acid (AA), immunoglobulin G (IgG) and prostate-specific antigen (PSA) were used as interfering substances for interference studies. As shown in Fig. S5, interference studies have shown that compared with detecting BNP the DPV and amperometric *i–t* curve induced changes in the current response were less than 5%, indicating that the immunosensor demonstrated eminent selectivity for the detection of BNP.

To investigate the reproducibility of the designed immunosensor, five modified electrodes were prepared for the detection of 1.0 pg/mL of BNP. As shown in Fig. S6, the relative standard deviation (RSD) of the measurements for modified electrodes were 4.6% (DPV) and 3.6% (amperometric *i–t* curve), suggesting that the fabricated immunosensor performed excellent the reproducibility and precision.

In order to evaluate the stability of the proposed immunosensor, a series of modified electrodes were prepared for the detection of 1.0 pg/mL of BNP and stored at 4 °C when not in use. As shown in Fig. S7, after one week, the DPV current response signal and the amperometric *i–t* curve of the immunosensor separate decreased 3.6% and 2.2%. After four weeks, the DPV current response signal and the amperometric *i–t* curve of the immunosensor separate decreased 9.8% and 9.2%, proving that the proposed immunosensor possessed good stability.

3.7. Real sample analysis

To evaluate the precision and reliability of the designed immunosensor for real sample analysis, the standard addition method was applied to investigate the recoveries of different concentrations for BNP in human serum samples. As shown in Table 1, the concentration of 5.0, 10.0 and 15 pg/mL for solution were respectively added into the human serum sample, the RSD ranged were 2.9–3.5% (DPV) and 2.6–3.3% (amperometric *i–t* curve), the recovery rate ranged were 97.0–102.1% (DPV) and 97.6–101.4% (amperometric *i–t* curve). As a result, the two parallel assays methods achieved consistent results on this platform which could be effectively applied to quantitative detection of the BNP levels in human serum samples.

4. Conclusions

In this work, the development of a dual mode competitive electrochemical immunosensor (DPV and amperometric *i–t* curve) for quantitative detection of BNP has reported by employing GS/SnO_2/PAN-Au as the matrix materials and $ZnCo_2O_4$/N-CNTs complex as the labels. Owing to the excellent electrical conductivity of GS/SnO_2/PAN-Au and the superior catalytic effect of $ZnCo_2O_4$/N-CNTs on H_2O_2, the immunosensor displayed a low detection limit, high sensitivity, good reproducibility, outstanding stability and excellent selectivity. The two parallel assays methods achieved consistent results on a single platform and provided a new promising alternative for the rapid determination of other biomarkers in clinical diagnosis.

Acknowledgments

This study was supported by the Natural Science Foundation of Shandong Province (No. ZR2016BM20), National Natural Science Foundation of China (Nos. 21575050, 21505051), National Key Scientific Instrument and Equipment Development Project of China (No. 21627809).

Appendix A. Supporting information

Supplementary data associated with this article can be found in the online version at doi:10.1016/j.bios.2018.11.009.

References

Acevedo, D.F., Rivarola, C.R., Miras, M.C., Barbero, C.A., 2011. Electrochim. Acta 56, 3468–3473.
Bera, S., Kundu, S., Khan, H., Jana, S., 2018. J. Alloy. Compd. 744, 260–267.
Choi, J.H., Lee, C., Cho, S., Moon, G.D., Kim, B.S., Chang, H., Jang, H.D., 2018. Carbon 132, 16–24.
de Ávila, B.E., Escamilla-Gómez, V., Campuzano, S., Pedrero, M., Pingarrón, J.M., 2013. Anal. Chim. Acta 784, 18–24.
Dong, W., Xu, J., Wang, C., Lu, Y., Liu, X., Wang, X., Yuan, X., Wang, Z., Lin, T., Sui, M., 2017. Adv. Mater. 29, 1700136.
Fan, L., Li, X., Yan, B., Feng, J., Xiong, D., Li, D., Gu, L., Wen, Y., Lawes, S., Sun, X., 2016. Adv. Energy Mater. 6, 1502057.
Han, Q., Wang, R., Xing, B., Chi, H., Wu, D., Wei, Q., 2018. Biosens. Bioelectron. 106, 7–13.
Hu, L., Zheng, J., Zhao, K., Deng, A., Li, J., 2017. Biosens. Bioelectron. 101, 260–267.
Jang, H.R., Wark, A.W., Baek, S.H., Chung, B.H., Lee, H.J., 2014. Anal. Chem. 86, 814–819.
Jin, Y., Jia, M., 2015. Colloid Surf. A. 464, 17–25.
Ke, W., Fang, G., Liu, Q., Xiong, L., Qin, P., Tao, H., Wang, J., Lei, H., Li, B., Wan, J., 2015. J. Am. Chem. Soc. 137, 6730–6733.
Kurita, R., Yokota, Y., Sato, Y., Mizutani, F., Niwa, O., 2006. Anal. Chem. 78, 5525–5531.
Lei, Y.M., Xiao, M.M., Li, Y.T., Xu, L., Zhang, H., Zhang, Z.Y., Zhang, G.J., 2017. Biosens. Bioelectron. 91, 1–7.
Li, F., Li, Y., Feng, J., Gao, Z., Lv, H., Ren, X., Wei, Q., 2018. Biosens. Bioelectron. 100, 512–518.
Li, Y., Zhang, Y., Jiang, L., Chu, P.K., Dong, Y., Qin, W., 2016. Sci. Rep. 6, 22694.
Liu, J., Fu, S., Yuan, B., Li, Y., Deng, Z., 2010a. J. Am. Chem. Soc. 132, 7279–7281.
Liu, L., Li, Y., Tian, L., Wei, Q., Cao, W., 2016a. Sens. Actuators B: Chem. 237, 733–739.
Liu, L., Tian, L., Zhao, G., Huang, Y., Wei, Q., Cao, W., 2017. Anal. Chim. Acta 986, 138–144.
Liu, R., Liu, J., Xie, L., Wang, M., Luo, J., Cai, X., 2010b. Talanta 81, 1016–1021.
Liu, Y., Zhang, Y., Wu, D., Fan, D., PANg, X., Zhang, Y., Ma, H., Sun, X., Wei, Q., 2016b. Biosens. Bioelectron. 86, 301–307.
Liu, Z.Q., Cheng, H., Li, N., Ma, T.Y., Su, Y.Z., 2016c. Adv. Mater. 28, 3777.
Ma, X., Zhang, P., Zhao, Y., Liu, Y., Li, J., Zhou, J.Y., PAN, X., Xie, E., 2017. Chem. Eng. J. 327, 1000–1010.
Mishra, A.K., Ramaprabhu, S., 2011. J. Phys. Chem. C. 115, 14006–14013.
Saito, Y., Nakao, K., Itoh, H., Yamada, T., Mukoyama, M., Arai, H., Hosoda, K., Shirakami, G., Suga, S., Minamino, N., 1989. Biochem Bioph. Res Co. 158, 360–368.
Serafín, V., Torrente-Rodríguez, R.M., González-Cortés, A., García, dF.P., Sabaté, M., Campuzano, S., Yáñez-Sedeño, P., Pingarrón, J.M., 2018. Talanta 179, 131–138.
Shiqiang, Yaping, Ding, Jiangjiang, Zhang, QingshengWu, Zongqian, 2017. Nano Res. 10, 1–13.
Si, Y., Samulski, E.T., 2008. Chem. Mater. 20, 6792–6797.
Song, H., Zhang, L., He, C., Qu, Y., Tian, Y., Lv, Y., 2011. J. Mater. Chem. 21, 5972–5977.
Tran, V.H., Khan, R., Lee, I.H., Lee, S.H., 2017. Sol. Energ. Mat. Sol. C. 179, 260–269.
Wang, J., Wang, X., Tang, H., Gao, Z., He, S., Li, J., Han, S., 2017a. Biosens. Bioelectron. 100, 1–7.
Wang, Y., Hu, L., Zhang, G., Yan, T., Yan, L., Wei, Q., Du, B., 2017a. J. Colloid Interface Sci. 494, 380–388.
Wang, Y., Ma, H., Wang, X., PANg, X., Wu, D., Du, B., Wei, Q., 2015. Biosens. Bioelectron. 74, 59–65.

Wang, Y., Zhao, G., Li, X., Liu, L., Cao, W., Wei, Q., 2018. Biosens. Bioelectron. 101, 290–296.
Wei, Y., Li, X., Sun, X., Ma, H., Zhang, Y., Wei, Q., 2017. Biosens. Bioelectron. 94, 141–147.
Wu, S., Su, F., Dong, X., Ma, C., PANg, L., Peng, D., Wang, M., He, L., Zhang, Z., 2017. Appl. Surf. Sci. 401, 262–270.
Xiong, Z., Wang, X., Lee, K., Zhan, X., Chen, Y., Tang, J., 2018. Acs Appl. Mater. Interfaces 10, 9211–9215.
Xu, D., Li, X., Zhang, D., 2014. Mater. Res. Bull. 59, 77–83.